Diffraction of H from LiF(001): From slow normal incidence to fast grazing incidence

A. S. Muzas, Fabien Gatti, F. Martin, C. Diaz

Diffraction of H from LiF(001): From slow normal incidence to fast grazing incidence

A.S. Muzas [a], F. Gatti [b], F. Martín [a,c,d], C. Díaz [a,d,*]

[a] Departamento de Química Módulo 13, Universidad Autónoma de Madrid, 28049 Madrid, Spain
[b] CTMM, Institute Charles Gerhardt, UMR 5253, Université de Montpellier II, place Eugéne Bataillon, 34009 Montpellier, France
[c] Instituto Madrileño de Estudios Avanzados en Nanociencia (IMDEA-nanociencia), Cantoblanco, 28049 Madrid, Spain
[d] Condensed Matter Physics Center (IFIMAC), Universidad Autónoma de Madrid, 28049 Madrid, Spain

Describing diffraction of atomic and molecular projectiles at fast grazing incidence presents a real challenge for quantum theoretical simulations due to the high incidence energy (100 eV–1 keV) used in experiments. This is one of the main reasons why most theoretical simulations performed to date are based on reduced dimensional models. Here we analyze two alternatives to reduce the computational effort, while preserving the real dimensionality of the system. First, we show that grazing incidence conditions are already fulfilled for incidence angles $\leqslant 5^{\circ}$, i.e., incidence angles higher than those typically used in experiments. Thus, accurate comparisons with experiment can be performed considering diffraction at grazing incidence, but with smaller total incidence energies, whilst keeping the same experimental normal energy in the calculations. Second, we show that diffraction probabilities obtained at fast grazing incidence are fairly well reproduced by simulations performed at slow normal incidence. This latter approach would allow one to simulate several experimental spectra, measured at the same normal incidence energy for several incidence crystallographic directions, with only one calculation. This approach requires to keep the full dimensionality of the system.

1. Introduction

Since 2007, when first diffraction experimental results obtained using grazing incidence fast atoms diffraction (GIFAD) techniques were published [1,2], these techniques have highly improved [3]. To present, they have been used to study a wide number of surfaces, including insulating [1,2,4], semiconductor [5] oxide [6–9], metal [10–13], and reconstructed surfaces [14], as well as superstructures adsorbed on metal surfaces [15–19], and even Graphene adsorbed on SiC(0001) [20]. This fruitful experimental effort has encouraged theorists to perform detailed quantum theoretical studies aiming to analyze and understand GIFAD experiments. However, these theoretical simulations present a major challenge due to the huge incidence energy used in the experiment.

In order to reduce the computational effort, and make the calculations feasible using reasonable computational resources, the axial surface channeling (ASC) approximation [5,24–26] and dynamics semi-quantum approaches [21–23] has been widely used. Within the ASC approximation, the dimensionality of the system is reduced to two-dimensions (2D) by considering that the projectile feels an average potential along the incidence direction. As already discussed in the literature [27,28] this approximation holds whenever the projectile feels a quasi-periodic potential and follows trajectories that are nearly parallel to the surface [29], i.e., whenever the condition $a \ll (E_i/tan\theta_i)/(dV_{3D}/dZ)$ is fulfilled [30] -a being the lattice constant, E_i and θ_i the incidence energy and polar angle, respectively, and dV_{3D}/dZ the variation of the three-dimensional potential over Z (see Fig. 1 for coordinates definition). Thus, this approximation may fail, for example, for surfaces with large lattice parameters, as recently shown for the case of diffraction of H atoms from the reconstructed (12×4) phase of the $Al_2O_3(11\bar{2}0)$ surface [8], whose experimental diffraction spectra displays several Laue circles revealing the three-dimensionality of the system.

In this work, using as benchmark system H/LiF(001), we have investigated how to reduce the computational effort required to study GIFAD phenomena, but keeping the full dimensionality of the system. When performing quantum dynamics calculations of atom(molecule)/surface systems using grid methods [31–33] the computational effort is fundamentally linked to the number of

* Corresponding author at: Departamento de Química Módulo 13, Universidad Autónoma de Madrid, 28049 Madrid, Spain.
E-mail address: cristina.diaz@uam.es (C. Díaz).

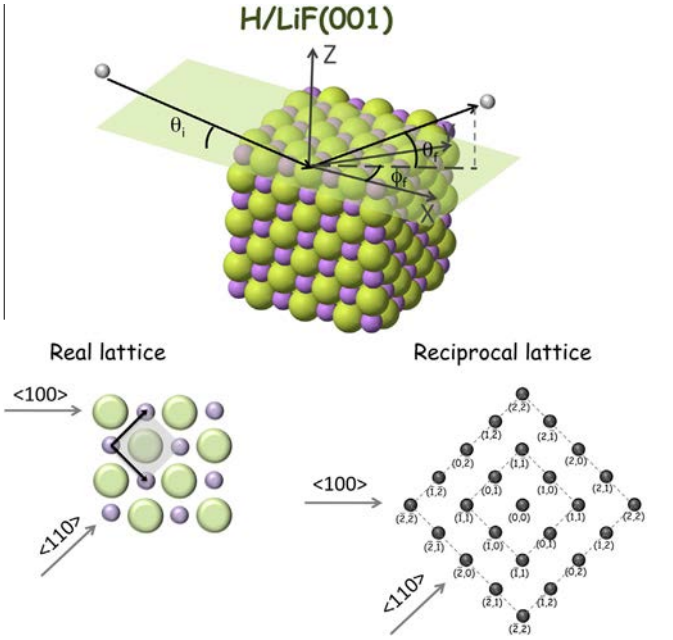

Fig. 1. Top: schematic representation of the H/LiF(100) system and the Cartesian coordinates system. Bottom: real and reciprocal lattices. Dashed gray lines show diffraction orders as defined in this work. Number within bracket indicate the incidence direction considered in this work.

basis functions required to describe accurately each degree of freedom (DOF): the higher the energy associated to a specific DOF the higher the number of basis functions needed to properly describe the motion along this DOF. In fact, we have estimated that GIFAD calculations at typical experimental conditions demand twice more RAM memory and ten times more CPU time than typical low energy diffraction calculations -within the Multi Configuration Time-Dependent Hartree (MCTDH) method framework (see below). These requirements could imply prohibitive calculations, for example, when molecular projectiles are involved. In order to reduce this computational effort, we have to take into account that GIFAD diffraction is mainly governed by the projectile low normal incidence energy (E_n), and that one can usually disregard the projectile total (E_i) and parallel (E_p) energies. Thus, the same diffraction spectra should be observed for a range of E_p's and polar incidence angles, θ_i (see Fig. 1), while keeping E_n constant. Of course, higher θ_i's imply lower E_p's, and therefore, lower computational effort. Our working hypothesis is that we can perform GIFAD calculations to much lower incidence energy that in experiment, and still be directly comparable with experimental results obtained at fast grazing incidence. In addition, with the aim of proposing a method to reduce the computation effort, while keeping the accuracy of the theoretical analysis, we have tested to what extend quantum calculations at slow normal incidence could be used to simulate GIFAD experiments and by extension GIFMD (grazing incidence fast molecules diffraction) experiments.

As we show below, our results indicate that grazing incidence conditions are reached at incidence angles higher than the ones used experimentally, and that results at slow normal incidence could be used, as a first approximation, to analyze fast grazing incidence experimental results. At this point, we should remark that the two methods we propose to save computing time do not represent *per se* a substantial improvement respect to the ASC approach, they just represent other approaches to the problem. In fact, our proposed approaches can be used within the same conditions for which the ASC approximation holds. However, to keep the full dimensionality of the system presents an advantage over this approach, namely, it allows one to analyze not only GIFAD and GIFMD experiments at low computational cost, but also quasi-GIFAD and quasi-GIFMD ones, similar to the ones published in Ref. [8]. Thus, the dynamics can be easily adapted according to the experimental conditions and/or the system we are interesting in. Furthermore, using slow normal incidence calculations to simulate grazing incidence results would allow one to simulate several diffraction spectra, measured at different crystallographic directions, with only one calculation. Of course, to take advantage of this latter method, we have to keep the full dimensionality of the system.

2. Theoretical approach

To perform our dynamics study, we have carried out quantum dynamics calculations by solving the time-dependent Schrödinger (TDS) equation for the nuclear Hamiltonian of the system. To solve the TDS equation we have made use of the Heiderberg MCTDH package [34,32,33,35], which has been already successfully used to study molecular reactive scattering from surface [36–39], and also diffraction of atoms from surfaces at low incidence energy [40]. Using the MCTDH method, we write the nuclear wave function of our 3D-system (see Fig. 1) as a sum of products of single-particle functions (SPFs),

$$\Phi(q_1,\ldots,q_f,t)=\sum_{j_1=1}^{n_1}\cdots\sum_{j_f=1}^{n_f}A_{j_1\ldots j_f}(t)\prod_{k=1}^{f}\varphi_{j_k}^{(k)}(q_k,t), \tag{1}$$

where f denote the number of degrees of freedom (DOFs), in our case three, q_i (i = 1,...,f) the ith nuclear coordinate, $A_{j_1\ldots j_f}$ the time-dependent expansion coefficients, $\varphi_{j_k}^{(k)}$ the time-dependent SPFs, and n_i the number of the SPFs used to describe each DOF. The SPFs are represented by linear combinations of time-independent primitive bases functions,

$$\varphi_{i_k}^{(k)}(q_k,t)=\sum_{i_k=1}^{N_k}C_{i_k j_k}^{(k)}(t)\chi_{i_k}^{(k)}(q_k), \tag{2}$$

where $\chi_{i_k}^{(k)}$ have been chosen as the basis functions of a Fast Fourier Transform (FFT) representation. At this point, it is worth pointing out that within this formalism the equations of motions for the expansion coefficients and the SPFs are derived from the Dirac–Frenkel variational principle, which leads to a set of coupled equations that can be solved with less computational effort than in standard time-dependent wave packet (TDWP) propagation methods. This is so because in the MCDTH method the nuclear wave function can be expanded in a smaller number of SPFs than the number of time-independent basis functions needed in a standard TDWP method.

Finally, to obtain diffraction probabilities, we have performed a flux analysis of the reflected wave function, which is absorbed by a complex absorbing potential placed in the non-interaction Z region. The main parameters used in the quantum calculations are listed in Table 1.

Dynamics simulations have been performed on a three-dimensional (3D) potential energy surface (PES) originally obtained by applying the corrugation reducing procedure (CRP) [41] to a set of density functional theory (DFT) energies (see Ref. [42] for a detailed description of the PES). However, from a computational point of view, the MCTDH method is more efficient when combined with PES's that have the form of sum of products of one-dimensional functions [47,32] such as:

$$V(q_1\ldots q_f)=\sum_{i=1}^{s}V_i(q_1)V_i(q_2)\ldots V_i(q_f) \tag{3}$$

Table 1
MCTDH calculation parameters as a function of the initial polar angle (θ_i). $N_{X,Y}$ and N_Z are the FFT primitive functions for coordinates X, Y and Z, respectively. See Fig. 1 for coordinates definition. Specific parameters used for incidence conditions $\theta_i \leqslant 2^\circ$ are given within brackets.

	$\theta_i \geqslant 5^\circ$ ($\leqslant 2^\circ$)
Initial wave packet	
Width, ΔZ_0 (Å)	0.5
Position, Z_0 (Å)	6.5
Grid parameter	
Type X, Y, Z	FFT
X, Y-range (Å)	0.0–11.52
$N_{X,Y}$	600 (1500)
Z-range (Å)	−0.75–15.0
N_Z	324 (500)
Complex absorbing potential	
Z-range (Å)	6.5–15.0
Strength (a.u.)	5.79×10^{-5}
SPFs per degree of freedom, X, Y, Z	9, 9, 9
Propagation time (fs)	450

To transform our 3D non-separable potential into a product of 1D functions, we have used the POTFIT procedure [43,44]. Within this procedure the PES of expanded in the so-called natural potentials, $v_j(q_i)$, as follow:

$$V^{approx}(q_1,\ldots,q_f) \approx \sum_{j_1}^{m_1}\sum_{j_f}^{m_f} C_{j_i\ldots J_f}\, v_{j_1}(q_1)\ldots v_{j_f}(q_f), \tag{4}$$

where $\{m_i\}$ represents a set of expansion orders. The expansion coefficients are determined by the overlaps between the primitive PES and the natural potentials as:

$$C_{j_i\ldots J_f} = \sum_{j_1}^{N_1}\sum_{j_f}^{N_f} V_{i_1\ldots i_f}\, v_{i_1 J_1}\ldots v_{i_f J_f}. \tag{5}$$

Parameters related to the POTFIT procedure and the accuracy of the approximated potential (V^{approx}) are given in Table 2.

3. Results and discussion

We have first analyzed the diffraction probabilities as a function of the incidence polar angle θ_i, while keeping the normal incidence energy constant. In Fig. 2, we show the evolution of the most intense diffraction peaks (see Fig. 1 for peak definition) with θ_i -in the case of symmetric peaks, only one of them is represented. From this figure, we can clearly see that specular peaks probabilities increases and diffraction peaks probabilities decrease with decreasing θ_i, and vanish at $\theta_i \approx 10^\circ$, except for peaks perpendicular to the incidence direction in the reciprocal space (see Fig. 1), the only ones observed at grazing incidence. The behavior of the latter peaks as a function of θ_i is also quite interesting, for the ⟨110⟩ incidence direction (the one shown in Fig. 2), we can see that the first order peaks probability [(0, 1) and (0, $\bar{1}$)] increases slightly with decreasing θ_i, while the probability of the second order peaks [(0, 2) and (0, $\bar{2}$)] remains almost constant. Similar results (not shown here) are obtained for the ⟨100⟩ direction: the first order peaks probability [(1, $\bar{1}$) and ($\bar{1}$, 1)] increases with decreasing θ_i and the second order peaks one [(2, $\bar{2}$) and ($\bar{2}$, 2)] remains constant. Once grazing incidence is reached (around $\theta_i = 5^\circ$), these survivor peaks, both the specular and the diffracted ones, remain constant. Interestingly, it should be noticed that, independently of the incidence direction, for incidence angles smaller than 20°. only the specular and the perpendicular diffraction peaks have a probability larger than zero, and that the diffraction spectra do not change significantly for θ_i below 5°, i.e., grazing incidence conditions seem to be reached for an initial polar angle around 5°. These results indicate that it is possible to compare experimental results obtained, for example, for $\theta_i = 1^\circ$. with theoretical ones obtained for $\theta_i = 5^\circ$ provided that E_n is the same. Thus, for example, an experiment performed at $E_i = 800$ eV and $\theta_i = 1.11^\circ$. could be described using theoretical simulations for $E_i = 40$ eV and $\theta_i = 5^\circ$. At this point, we should remark that to the best of our knowledge no GIFAD experimental results for $\theta_i \geqslant 2.5^\circ$ are available in the literature. Lienemann et al. [45] have shown that, for H/LiF(001) at E_i = 1.0 keV, incoherent scattering due to electronic excitations clearly dominate for $\theta_i \geqslant 1.5^\circ$. But, in this experiment, E_i was kept fixed, while E_n increased with θ_i. However, no systematic experimental study keeping E_n constant and varying θ_i, aiming to find the maximum θ_i angle that defines grazing incidence, has ever been performed. We hope that our analysis will encourage such experimental study.

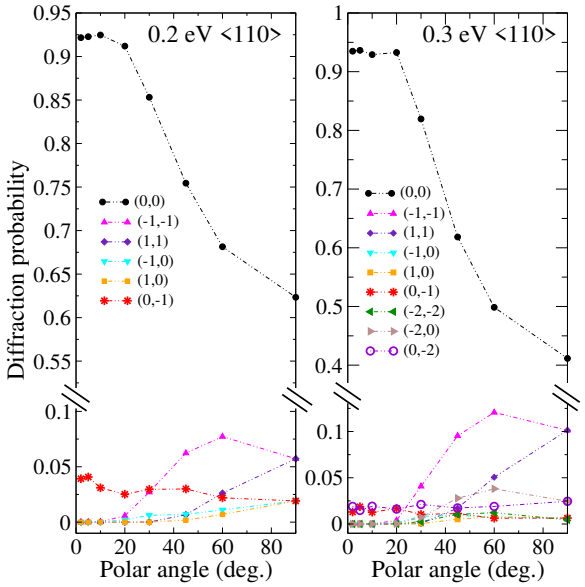

Fig. 2. Diffraction probabilities as a function of the polar incidence angles (θ_i) along the crystallographic direction ⟨110⟩, for the most intense diffraction peaks obtained in the simulations. Notice that for the lower incidence angles only peaks perpendicular to the crystallographic direction ⟨110⟩, i.e., peaks of the form (0, n), are populated (see Fig. 1).

Table 2
Parameters used to represent the H/LiF(001) PES in a suitable form for the MCTDH equations of motion using the POTFIT algorithm. Δ^w_{rms} and Δ^{rw}_{rms} represent the rms error on all grid points and on relevant grid points, respectively. max(ϵ) and max(ϵ^r) represent the maximum error on all grid points and on relevant grid points, respectively.

Natural potential basis	
N_x, N_y	25, 25
N_z	Contr [47]
Relevant region of the fit	
Z (Å)	>0.5
V (eV)	<3
POTFIT accuracy	
N_{iter}	4
Δ^{rw}_{rms}, Δ^w_{rms} (meV)	0.15, 5.03
max(ϵ^r), max(ϵ) (meV)	4.54, 306

For the sake of completeness, we have compared our theoretical results with experimental data available in the literature. In Fig. 3, we compare experimental results from Ref. [46] with our theoretical results, obtained for $\theta_i = 5^\circ$. From this Fig., we can see that our results reproduce qualitatively the experimental observations. In

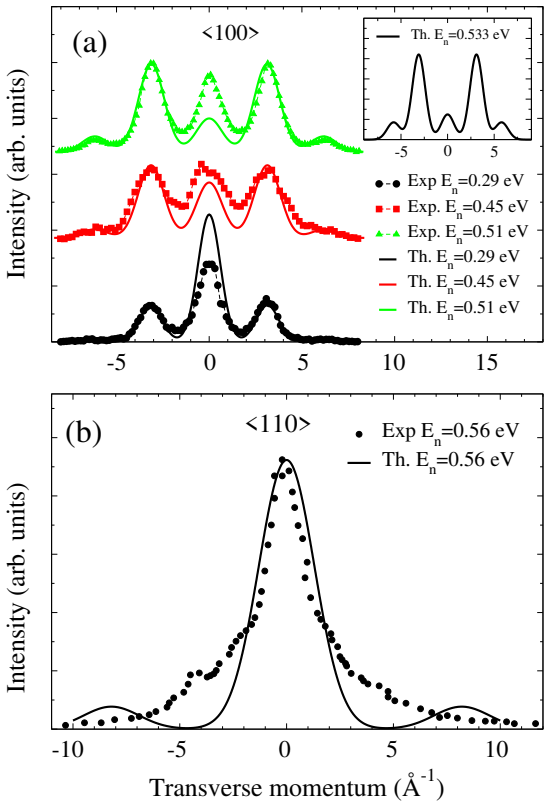

Fig. 3. Diffraction spectra of H/LiF(001) along the ⟨100⟩ (a) and ⟨110⟩ (b) crystallographic directions. Black stars: experimental data from Ref. [46]. Solid lines: quantum theoretical results ($\theta_i = 5^\circ$), which have been convoluted with a 1D Gaussian function to simulate the experimental resolution. The inset show the theoretical diffraction spectrum for E_n = 0.533 eV.

particular, theoretical spectra display, in agreement with experiment, high first order diffraction peaks along the ⟨100⟩ direction, and a clear predominance of the specular peak along the ⟨110⟩ one. A closer look to Fig. 3(a) reveals some disagreement between theory and experiments. The experimental spectrum show first order diffraction peaks more intense than the specular one, whereas the simulated one display a more intense specular peak. However, as also shown in Fig. 3(a), if we increase the normal energy in our simulations the first order peaks increase and the specular one decreases. In fact, as shown in the inset of this Fig., for high enough normal energies, we recover the experimental trend. Thus, from this analysis, we can conclude that out quantum theoretical results reproduce the experimental ones with a energy shift. Similar agreement with experiments has been previously obtained using a classical binning method and the same PES [42]. Interestingly, we should also point out that the diffractogram shown in the inset of Fig. 3 agrees with the 2D diffraction pattern recorded by Winter et al. [3] for the same incidence normal energy. Here, we should also point out that the disagreements found between theory and experiment, are most likely due, beyond experimental uncertainties, to the accuracy of the DFT functional used in computing the single point configurations energies needed to built the PES. Here, we have not performed a systematic search for the functional reproducing best the experimental measurements because, on the one hand, there are not enough experimental measurements to carried out properly this search (see Ref.[48,49]), and on the other hand, it was no the aim of this study to reproduce a particular experiment, but to carry out an analysis that could be extrapolated to any system, even a to fictitious one.

Finally, we have also performed a comparison between the spectra obtained at fast grazing incidence and the spectra that it would be obtained at normal incidence if only the peaks populated at fast grazing incidence were considered, i.e., if only the peaks perpendicular to the crystallographic incidence direction were considered. In Fig. 4 we show such comparison along two crystallographic incidence directions, ⟨100⟩ and ⟨110⟩, for several normal incidence energies. As we are only interested in relative intensities, in Fig. 4, we have renormalized the probability of the normal incidence peaks to the probability of the specular peak obtained at fast grazing incidence. From this figure, we can extract several interesting conclusions: (i) for the lower normal energies, for which only the first order peaks have a significantly intensity, spectra at normal and grazing incidence almost overlap. For higher normal energies, when second order peaks start to show up, the quantitative agreement between both spectra gets a little worse. (ii) The variation of the spectrum at fast grazing incidence as a function of E_n is qualitatively well reproduced by normal incidence simulations. For example, the decrease of the first order peaks and the increase of the second order ones along the ⟨110⟩ direction, obtained at fast grazing incidence, is well reproduced by a normal incidence simulation, although at normal incidence second-order peaks are populated faster than at fast grazing incidence. This worsen of the agreement between normal and grazing incidence results (for a fixed θ_i) when the normal energy increases, it is related to the deterioration of the grazing incidence conditions. A more quantitative analysis of our results can be performed from the relative intensities of the different diffraction peaks, as they come out from the simulations, listed in Table 3.

The latter results have important implications from the simulation point of view. They show that with a single normal incidence

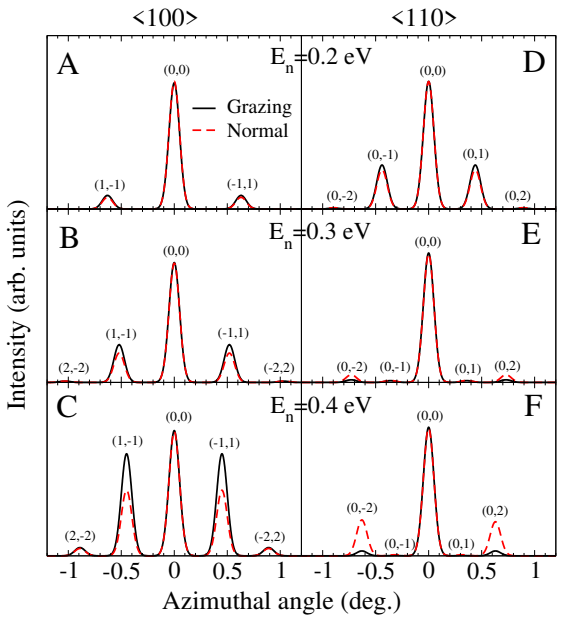

Fig. 4. Comparison between simulated diffraction spectra at grazing incidence, $\theta_i = 2^\circ$ and E_i = 164 eV (A and D) 246 eV (B and E), 328 eV (C and F), and at normal incidence, $\theta_i = 90^\circ E_i = E_n$; for several normal incidence energies and two crystallographic incidence directions.Note that in the case of normal incidence, we have only included in the spectra the diffraction peaks perpendicular to the crystallographic incidence directions corresponding to the fast grazing incidence calculation. i.e., we have included peaks of the form (±m,∓m) for the incidence direction ⟨100⟩, and of the form (0,±n) for the ⟨110⟩ one (see Fig. 1). Normal-incidence diffraction peaks have been renormalized to the specular peak obtained at grazing incidence (see text). Delta-functions theoretical diffraction distributions have been convoluted with 1D Gaussian functions of width $\sigma = 0.05$ to simulate the experimental resolution.

Table 3
Theoretical relative intensities used to draw spectra shown in Fig. 4.

E_z (eV)	0.2 Nor. Graz.	0.3 Nor. Graz.	0.4 Nor. Graz.
⟨100⟩			
$I_{(2,-2)}/I_{(0,0)}$	0.001 0.001	0.011 0.011	0.059 0.066
$I_{(1,-1)}/I_{(0,0)}$	0.092 0.108	0.246 0.315	0.527 0.815
⟨110⟩			
$I_{(0,1)}/I_{(0,0)}$	0.031 0.035	0.015 0.014	0.008 0.009
$I_{(0,2)}/I_{(0,0)}$	0.010 0.007	0.060 0.020	0.281 0.027

energy simulation, which requires much less computational resources than a fast grazing incidence calculation, we can simulate reasonably well the diffraction spectra obtained at grazing incidence, at a given normal incidence energy, along any incidence direction. In other words, by just performing a single *cheap* calculation, one can simulate reasonable well several experimental conditions.

4. Summary

We have performed MCTDH quantum dynamics calculations, based on a first-Principles 3D potential energy surface, aimed at evaluating several options to reduce the computational effort required to analyze experimental spectra obtained at fast grazing incidence conditions. Taking H/LiF(001) as a benchmark system, we have shown that grazing incidence conditions are fulfilled at incidence polar angles ($\theta_i \approx 5^\circ$) higher than the ones typically used in experiments, i.e., we have shown that, for a given normal incidence energy, the same results can be obtained by using lower total energies than those used in experiment. We have also shown that diffraction at normal incidence can be used, at a first approximation, to simulate fast grazing incidence, simply by analyzing diffraction peaks perpendicular to the crystallographic incidence direction considered in each specific experiment. Thus, one single *cheap* calculation at normal energy could be used to simulate diffraction spectra measured in GIFAD and GIFMD experiments along several incidence directions and angles. Although here, we have to take into account that the ability of normal incidence simulations to reproduce grazing incidence results worsen when the normal incidence energy increases.

Finally, we should point out that the two approximations analyzed here, are valid within the same incidence conditions as the ASC approximation. However, to keep the full dimensionality of the system presents some advantages: (i) one can used the same potential and dynamics method to analyze both GIFAD (GIFMD) and quasi-GIFAD (quasi-GIFMD) experiments; (ii) one can used only one slow normal incidence calculation to simulate several experiments carried out, at the same normal incidence, for several crystallographic directions.

Acknowledgements

We thank BSC-RES and CCC-UAM for allocation of computer time. Work partially supported by the MICINN Projects Nos FIS2013-42002-R and CTQ2013-50150-EXP, and the CAM project No. S2013/MIT-2850. C. Díaz acknowledges the Ramón y Cajal program, and A.S. Muzas the FPI program of the MICINN.

References

[1] A. Schüller, S. Wethekam, H. Winter, Phys. Rev. Lett. 98 (2007) 016103-1.
[2] P. Rousseau, H. Khemliche, A.G. Borisov, P. Roncin, Phys. Rev. Lett. 98 (2007) 016104-1.
[3] H. Winter, A. Schüller, Prog. Surf. Sci. 86 (2011) 169.
[4] U. Specht, M. Busch, J. Seifert, H. Winter, K. Gärtner, R. Wlodarczyk, M. Sierka, J. Sauer, Nucl. Instrum. Meth. Phys. Res. B 269 (2011) 799.
[5] M. Debiossac, A. Zugarramurdi, H. Klemliche, P. Rocin, A.G. Borisov, A. Momeni, P. Atkinson, M. Eddrief, F. Finocchi, V.H. Etgens, Phys. Rev. B 90 (2014) 155308.
[6] M. Busch, J. Seifert, E. Meyer, H. Winter, Phys. Rev. B 86 (2012) 241402.
[7] A. Schüller, D. Blauth, J. Seifert, M. Busch, H. Winter, K. Gärtner, R. Wlodarczyk, J. Sauer, M. Sierka, Surf. Sci. 606 (2012) 161.
[8] M. Busch, J. Seifert, E. Meyer, H. Winter, Nucl. Instrum. Methods Phys. Res. B 317 (2013) 90.
[9] M. Busch, E. Meyer, K. Irmscher, Z. Galazka, K. Gärtner, H. Winter, Appl. Phys. Lett. 105 (2014) 051603.
[10] M. Busch, A. Schüller, S. Wethekam, H. Winter, Surf. Sci. 603 (2009) L23.
[11] P. Tiwald, A. Schüller, H. Winter, K. Tökesi, F. Aigner, S. Gräfe, C. Lemell, J. Burgdörfer, Phys. Rev. B 82 (2010) 125453.
[12] J. Seifert, A. Schüller, H. Winter, R. Wlodarczyk, J. Sauer, M. Sierka, Phys. Rev. B 82 (2010) 035436.
[13] C.A. Ŕos-Rubiano, G.A. Bocan, M.S. Gravielle, N. Bundaleski, H. Khemliche, P. Rocin, Phys. Rev. A 87 (2013) 012903.
[14] H. Khemliche, P. Rousseau, P. Roncin, V.H. Etgens, F. Finocchi, Appl. Phys. Lett. 95 (2009) 151901.
[15] J. Seifert, H. Winter, Surf. Sci. 603 (2009) L109.
[16] A. Schüller, M. Busch, J. Seifert, S. Wethekam, H. Winter, K. Gärtner, Phys. Rev. B 79 (2009) 235425.
[17] J. Seifert, H. Winter, Phys. Rev. Lett. 108 (2012) 065503.
[18] J. Seifert, M. Busch, E. Meyer, H. Winter, Phys. Rev. Lett. 111 (2013) 137601.
[19] J. Seifert, M. Busch, E. Meyer, H. Winter, Phys. Rev. B 89 (2014) 075404.
[20] A. Zugarramurdi, M. Debiossac, P. Lunca-Popa, A.J. Mayne, A. Momeni, A.G. Borisov, Z. Mu, P. Roncin, H. Klemliche, Appl. Phys. Lett. 106 (2015) 101902.
[21] M.S. Gravielle, J.E. Miraglia, Phys. Rev. A 78 (2008) 022901.
[22] M.S. Gravielle, A. Schüller, H. Winter, J.E. Miraglia, Nucl. Instrum. Meth. Phys. Res. B 269 (2011) 1208.
[23] M.S. Gravielle, J.E. Miraglia, Phys. Rev. A 90 (2014) 052718.
[24] F. Aigner, N. Simonović, B. Solleder, L. Wirtz, J. Burgdörfer, Phys. Rev. Lett. 101 (2008) 253201.
[25] A. Schüller, S. Wethekam, D. Blauth, H. Winter, F. Aigner, N. Simonović, B. Solleder, J. Burgdörfer, L. Wirtz, Phys. Rev. A 82 (2010) 062902.
[26] A. Zugarramurdi, M. Debiossac, P. Lunca-Popa, L.S. Alarcon, A. Momeni, H. Khemliche, P. Rocin, A.G. Borisov, Phys. Rev. A 88 (2013) 012904.
[27] A. Zugarramurdi, A.G. Borisov, Phys. Rev. A 86 (2012) 062903.
[28] A. Zugarramurdi, A.G. Borisov, Nucl. Instrum. Meth. Phys. Res. B 317 (2013) 83.
[29] M. Debiossac, P. Roncin, Phys. Rev. A 90 (2014) 054701.
[30] D. Farías, C. Díaz, P. Nieto, A. Salin, F. Martín, Chem. Phys. Lett. 390 (2004) 250.
[31] G.J. Kroes, Prog. Surf. Sci. 60 (1999) 1.
[32] H.D. Meyer, G.A. Worth, Theor. Chem. Acc. 109 (2003) 251.
[33] H.D. Meyer, F. Gatti, G.A. Worth, Multidimensional Quantum Dynamics: MCTDH Theory and Applications, Wiley-VCH, Weinheim, 2009.
[34] M.H. Beck, A. Jäckle, G.A. Worth, H.D. Meyer, Phys. Rep. 324 (2000) 1.
[35] G.A. Worth, M.H. Beck, A. Jäckle, H.D. Meyer, The MCTDH Package, version 3.4 (2007). See <http://mctdh.unidh.de/>.
[36] R. van Harrevelt, Uwe Manthe, J. Chem. Phys. 121 (2004) 3829.
[37] C. Crespos, H.D. Meyer, R.C. Mowrey, G.J. Kroes, J. Chem. Phys. 124 (2006) 074706.
[38] G.J. Kroes, H.D. Meyer, Chem. Phys. Lett. 440 (2007) 334.
[39] G.P. Krishnamohan, R.A. Olsen, G.J. Kroes, F. Gatti, S. Woittequand, J. Chem. Phys. 133 (2010) 144308.
[40] M. Del Cueto, A.S. Muzas, G. Füchsel, F. Gatti, F. Martín, C. Díaz, Phys. Rev. B 93 (2016) 060301(R).
[41] H.F. Busnengo, A. Salin, W. Dong, J. Chem. Phys. 112 (2000) 7641.
[42] A.S. Muzas, F. Martín, C. Díaz, Nucl. Instrum. Meth. Phys. Res. B 354 (2015) 9.
[43] A. Jäckle, H.D. Meyer, J. Chem. Phys. 104 (1996) 7974.
[44] A. Jäckle, H.D. Meyer, J. Chem. Phys. 109 (1998) 3772.
[45] J. Lienemann, A. Schüller, D. Blauth, J. Siefert, S. Wethekam, M. Busch, K. Maass, H. Winter, Phys. Rev. Lett. 106 (2011) 067602-1.
[46] P. Rousseau, H. Khemliche, N. Bundaleski, P. Soulisse, A. Momeni, P. Rocin, J. Phys. Conf. Ser. 133 (2013) 012013.
[47] M.H. Beck, A. Jäckle, G.A. Worth, H.D. Meyer, Phys. Rep. 324 (2000) 1.
[48] C. Díaz, E. Pijper, R.A. Olsen, H.F. Busenengo, D.J. Auerbach, G.J. Kroes, Science 326 (2009) 832.
[49] M. Wijzenbroek, G.J. Kroes, J. Chem. Phys. 140 (2014) 084702.